Supporting Information for:

^{14}C-labelled nanoplastics reveal size-dependent bioaccumulation in Juvenile Rainbow Trout (*Oncorhynchus mykiss*)

Maya Al-Sid-Cheikh[*,a,f], Joyce W. L. Ang[b], Gareth T. W. Law[b], Ana Isabel Catarino[c,g], Theodore B. Henry[c], Steve J. Rowland[d], Marc-Andre Cormier[e,h], Richard C. Thompson[a]

[a] School of Biological and Marine Sciences, University of Plymouth, Drake Circus, Plymouth, PL4 8AA, United Kingdom

[b] Radiochemistry Unit, Department of Chemistry, Faculty of Science, University of Helsinki, A.I. Virtasen Aukio 1, P.O. Box 55, Helsinki, FI-00014, Finland

[c] School of Geography, Earth and Environmental Sciences, University of Plymouth, Drake Circus, Plymouth, PL4 8AA, United Kingdom

[d] Institute of Life and Earth Sciences Heriot-Watt University, John Muir Building, Edinburgh, EH14 4AS, United Kingdom

[e] Department of Earth Sciences, University of Oxford, South Parks Road, Oxford, OX1 3AN, United Kingdom

Corresponding Author

* Dr Maya Al Sid Cheikh, EaStCHEM School of Chemistry, University of Edinburgh, Joseph Black Building, Edinburgh, EH9 3FJ, United Kingdom. malsid@ed.ac.uk, phone: (+44)1316504764

Present/permanent Addresses

[f] EaStCHEM School of Chemistry, University of Edinburgh, Joseph Black Building, Edinburgh, EH9 3FJ, United Kingdom.

[g] Flanders Marine Institute (VLIZ), Research Division, Ocean and Human Health, InnovOcean Campus, Jacobsenstraat 1, 8400 Oostende, Belgium

[h] School of Geographical & Earth Sciences, University of Glasgow, Main Building, Glasgow, G12 8QQ, United Kingdom

This PDF file includes:

Table of Contents

Text S1: Radiosynthesis and Characterisation of [^{14}C]*n*PS

The particles used in this study were synthesised and fully characterised as described in Al-Sid-Cheikh et al. (2020); a brief summary is provided below.

Radiotracer and chemicals. Two batches of styrene [methylene-^{14}C] in hexane (specific activity 2.22 GBq mmol^{-1}; 0.58 MBq mg^{-1} or 0.63 MBq mg C^{-1}, molecular weight = 106.14 g mol^{-1}, American Radiolabeled Chemicals Inc.) was used as received for polymerisation into two batches of spherical polystyrene nanoparticles via micro-emulsion following the procedure of Al-Sid-Cheikh et al (2020). The micro-emulsion syntheses used sodium dodecyl sulfate (SDS, ≥99%, Alfa Aesar™), potassium persulfate (KPS, ≥99%, ACS reagent) and sodium hydroxide (NaOH, ≥98%) accordingly to the size of the particle. Water used in synthesis was purified with a Milli-Q® Integral Water Purification System for Ultrapure Water (18.2 MΩ cm^{-1}).

Radiolabelling procedure.

***[^{14}C]n*PS$_{20}$:** Radiolabelled 20 nm *n*PS ([^{14}C]*n*PS$_{20}$) was prepared using a conventional emulsion system with styrene 1 wt%, SDS 2 wt%, water 90.20 wt%, and KPS 3.60 mM. The vial was purged with nitrogen gas and then heated at 70°C for 24 hours.

***[^{14}C]n*PS$_{250}$:** Radiolabelled 250 nm *n*PS ([^{14}C]*n*PS$_{250}$) was prepared by surfactant-free emulsion polymerisation. The initiator solution was prepared separately with KPS 14.6 mM in the final water phase, NaOH 56.7 mM in the final water phase, and Milli-Q water 17 wt% mixed in a glass vial. Styrene 1 wt% and Milli-Q water 59 wt% were mixed at room temperature. The headspace inside the flask was then purged with nitrogen. The reaction was maintained at 70 °C under stirring for 24 h.

For both syntheses, unreacted monomer was removed by ultrafiltration (exclusion size of membrane: 30,000 g mol^{-1} cutoff).

Particle characterisation

Size & morphology. Transmission electron microscopy analyses provided a size characterization of 24.8 ± 12.8 and 248 ± 21 nm, both (n > 100) (Al-Sid-Cheikh et al., 2020). The particles were observed to have spherical shapes and rough surfaces: images are provided in Al-Sid-Cheikh et al., (2020).

Surface charge. At pH 6 in a sodium chloride solution (5 mM), the ξ-potentials of the particles were measured to be −129 ± 10 mV and −83.6 ± 11.9 mV for the 20 nm and 250 nm NPs, respectively (Al-Sid-Cheikh et al., 2020). These measurements were conducted using dynamic light scattering (DLS) with a dedicated Zetasizer (Malvern Panalytical®).

***Composition*.** Additional characterization techniques, namely Fourier-transform infrared spectroscopy (FTIR) and Raman spectroscopy, were employed (Figure S1). The FTIR analyses were conducted using an attenuated total reflection (ATR) crystal (Spectrum Two, PerkinElmer, UK). Prior to analysis, the samples were dried to prevent water bands in the spectrum. Powders were placed onto the ATR crystal, and the infrared spectra were recorded using a resolution of 4 cm^{-1} with 16 scans for each spectrum in the spectral range 4000 to 400 cm^{-1}. For Raman spectroscopy (InVia Reflex Raman Microscope, Renishaw, UK), dry particle powders were analysed using a 785 nm laser excitation (near-IR line laser, 100% laser power) and a 50XL objective. These analyses confirmed that the synthesized particles are indeed composed of polystyrene only.

Text S2: QWBA Calibration and Validation

Preparation of ^{14}C Standards and Calibration Curves. Quantification of [^{14}C] activity in quantitative whole-body autoradiography (QWBA) was achieved through calibration against external and internal standards.

At the *University of Helsinki*, calibration standards were prepared from ^{14}C-labelled poly(methyl methacrylate) (PMMA) polymers of known specific activity (1–10^7 kBq mL^{-1}), synthesised by polymerising ^{14}C-methyl methacrylate solutions using azobisisobutyronitrile (0.25% m/m) as a thermal initiator. Each ^{14}C-PMMA standard was polished and verified by liquid scintillation counting (LSC).

At the *Applied RadiIosotope & Environmental Laboratory* (ARIEL), calibration solutions were prepared by spiking 5 mL aliquots of a carboxymethylcellulose (CMC)/serum mixture with known activities of ^{14}C (10–1000 Bq g^{-1}). Each solution was homogenised for 30 min on a magnetic stirrer, and activities were verified in triplicate using a Hidex 300SL counter (10 min per replicate). Calibrator aliquots were frozen into a 2.5% CMC block, drilled with 6.5 mm cavities, refrozen, and sectioned (30 µm thickness) following standard QWBA procedures. The calibration standards were sectioned and exposed simultaneously with the fish samples to generate calibration curves.

Linear calibration curves were constructed by plotting digital light units per mm^2 (DLU mm^{-2}) or counts s^{-1} mm^{-2} against known ^{14}C concentrations. The limits of detection (LOD) and quantification (LOQ) were determined as 3.3 × and 10 × the standard deviation of the intercept, respectively. The resulting method exhibited high linearity over four orders of magnitude, with LOD = 3.31 ng $g_{w.w}^{-1}$. and LOQ = 10.1 ng g^{-1} w.w. for phosphor screen autoradiography (7-day exposure). The coefficient of variation was 16–18% for activities > 100 Bq $g_{w.w}^{-1}$ and 20–25% near the LOD/LOQ thresholds.

Image Acquisition Parameters. Tissue sections were exposed for 7 days to imaging plates (BAS-IP TR 2040 E; 20 × 40 cm; Fujifilm, Japan) in a lead-shielded box to minimise background radiation. The imaging plates were scanned using a Fujifilm FLA-5100 (University of Helsinki) or a GE Typhoon FLA 9000 (ARIEL) at 25 µm resolution (1016 dpi). The imaging systems were calibrated prior to each acquisition using internal phosphor screen standards.

Quantitative image analysis was performed with AIDA v5.0 SP 3 (Elysia-Raytest GmbH, Germany) and validated independently with ImageJ v1.53k (NIH, USA). Image processing parameters (brightness, contrast, and background correction) were kept constant across all samples to ensure quantitative consistency.

Cross-Validation with the BeaQuant System

***Cross-referencing Between Autoradiography Techniques*.** Real-time autoradiography acquisitions (BeaQuant) of selected *O. mykiss* sections were utilized as a reference to validate the data obtained from phosphor screen autoradiographs, ensuring data reliability (Figure S3, Text S1 Ang et al., 2023). The reduction in background noise observed in the BeaQuant system can be attributed to its higher limit of detection (LOD), as outlined in Table S2 (32.9 ng $g_{w.w.}^{-1}$), approximately 1 order of magnitude higher than the phosphor imager (FLA 9000 and FLA-5100) with LODs of 3.31 and $9.53 \cdot 10^{-1}$ ng $g_{w.w.}^{-1}$, respectively. As a result, the phosphor imager, capable of accumulating radiation over 7 or 16 days, demonstrates an improved ability to visualize finer structural details when compared to the BeaQuant system, given its lower LOD. The distribution of ^{14}C within the tissue remained consistent across both methodologies.

***Atmospheric background contribution*.** To ensure accurate spatially resolved quantification of [^{14}C]*n*PS, we investigated the background contribution from atmospheric ^{14}C uptake by the fish. The rainbow trout ^{14}C activity concentrations were estimated with the 2018 annual mean atmospheric ^{14}C specific activity of 14.05 dpm per gram of carbon. This consistency confirms that the signal recorded using the phosphor

screen autoradiography method indeed originated from the fish section samples and was not predominantly attributed to background noise.

***Variation in Organ Material: Effect on Detection*.** Only a fraction of electrons emitted (F_E) from ^{14}C decay within samples reaches the detector to be measured by autoradiography. F_E depends on both the sample density and chemical composition. As a result, it is anticipated that within the fish sample, with varying densities and composition among its organs, F_E might be different, potentially leading to the inaccurate representation of each organ's actual radioactivity. Monte Carlo simulations of ^{14}C emissions from various fish organs (differing density and chemical compositions, Table S3) were carried out with a GEANT4 (GEometry ANd Tracking, version 4.10.07) toolkit to investigate the emission fraction (F_E) (Agostinelli et al., 2003). Here we assumed homogeneous distribution of ^{14}C over a volume of a 1 mm × 1 mm × 30 μm organ section. With this fixed sample geometry and the varying simulated organ material, we calculated F_E by taking the ratio of electrons entering the detector to the total electrons emitted from the sample through ^{14}C radiation decay. The fish organs were simulated with analogous materials summarized in Tables S2 and S4. One million decay events were set for each organ simulation.

QWBA with real-time autoradiography: the BeaQuant System.

The BeaQuant system is a real-time autoradiography technique which uses micro-pattern gas detectors with a parallel ionization multiplier structure[1]. This technique provides faster and a more accurate data for samples with low radioactivity, which is suitable in the detection of low environmentally relevant levels of radiolabelled nanopolystyrene particles ([^{14}C]*n*PS) distributed within a rainbow trout (*Oncorhynchus mykiss*) tissue section.

Since the BeaQuant system directly records the data as counts/second/area (instead of phosphor screen autoradiography which requires the conversion from photostimulated luminescence to activity), the quantification is more precise. For example, a limited number of 100 detected beta particles within an organ section provides a standard error of 10% (Poisson noise), which is reasonable for biological studies. As a result, the BeaQuant is a faster method than phosphor screen autoradiography. In this study, the BeaQuant acquisition took 5 days to produce analyzable data, whereas phosphor screen autoradiography required a total of 7 days of exposure.

In quantitative whole-body autoradiography (QWBA) with small particles, a good spatial resolution is important to accurately distinguish the localization of the particles within the individual organ tissues. For the BeaQuant system, the spatial resolution for the detection of ^{14}C was reported as 35 μm^2. This spatial resolution is good in comparison to the average section length (head to tail) of the *O. mykiss* studied (14 ± 1 cm).

The BeaQuant allows for a lower background radioactivity contribution to the data compared to phosphor screen autoradiography. Due to the low density and thickness of the active gas media used (90% neon and 10% carbon dioxide gas in 1.1×10^5 Pa), the BeaQuant is largely insensitive to gamma radiation. Hence, there is less background cosmogenic radiation contribution picked up by the detector. In addition, the detector itself is shielded from external radiation sources.

For longer acquisition times (i.e., 1 to 2 weeks) required in low radioactive samples, classic phosphor screen autoradiography will experience the phenomena of "fading", whereby some of the alkali halide crystals in the imaging plate inevitably de-excites during exposure, leading to an inaccurate (underestimated) measurement of radioactivity[3]. The BeaQuant system does not face this problem.

In view of the above, we utilized the BeaQuant results as a form of quality control and benchmark to ensure that the data acquired from phosphor screen autoradiography is accurate for the purpose of this study.

Background Contribution from Atmospheric ^{14}C. To estimate the background ^{14}C contribution from the rainbow trout, we use the 2018 annual mean atmospheric ^{14}C specific activity of 14.05 dpm per gram of carbon[4]. The background ^{14}C activity concentration A (Bq g^{-1}) found in the rainbow trout can be calculated using equation S3,

$$A = S \cdot f_c \tag{S3}$$

where S =14.05 dpm per gram of carbon and f_c is the mass composition of carbon in the fish.

To ensure that the background contribution is not an underestimate, we take the maximum f_c value, which is the mass composition of carbon found in the oesophagus (0.187) with reference to Supplementary Table S4. Substituting these values into equation S3, the average background ^{14}C activity concentration for the rainbow trout sample is calculated to be $4.38 \cdot 10^{-2}$ Bq g^{-1}.

Based on our results, we found that the total ^{14}C specific activity for 27 rainbow trout samples were between 2.5 to 423.5 Bq $g_{\text{w.w.}}^{-1}$. Since the measured activity is higher than the background radiation, we have demonstrated that the measured radioactivity was real, and not solely due to background ^{14}C radiation. In fact, we note that the atmospheric background contribution is not significant (only constitutes 1.75% of the total rainbow trout radioactivity for the lowest detected activity). In addition, the experiments included the measurements of controls (rainbow trout with no ingestion of ^{14}C-radiolabelled nanopolystyrene), which did not display any signals in the QWBA results.

Conversion of ^{14}C Activity Concentrations to [^{14}C]nanopolystyrene Particle Concentrations

In this study, radiometric detection methods (liquid scintillation counting and quantitative whole-body autoradiography) were used to quantify the amount of [^{14}C]*n*PS accumulated and translocated within the rainbow trout. Hence, it is important to convert the measured ^{14}C activity concentrations, with respect to the wet weight of fish tissue (kBq $g_{\text{w.w.}}^{-1}$), to particle concentrations, in terms of nanograms of particles per gram of fish tissue (ng $g_{w.w.}^{-1}$), and number of particles per gram of fish tissue (wet weight).

For the conversion to ng $g_{\text{w.w.}}^{-1}$, we divide the ^{14}C activity concentration in the fish by the ^{14}C activity concentration in [^{14}C]*n*PS, as shown in equation (S1):

$$C_{\text{mass}}\ [\text{ng}\ g_{\text{w.w.}}^{-1}] = \frac{A_f\ [\text{kBq}\ g_{w.w.}^{-1}]}{A_p\ [\text{kBq}\ ng_{w.w.}^{-1}]} \tag{S1}$$

where C_{mass} is the mass/mass concentration of [^{14}C]*n*PS to the wet weight of the fish tissue, A_f is the activity concentration of ^{14}C detected in the fish tissue (derived from the detector measurements), and A_p is the activity concentration of ^{14}C in the radiolabelled nanopolystyrene particles, which is $2.11 \cdot 10^{-2}$ kBq $ng_{\text{w.w.}}^{-1}$.

To convert this to the number of particles per gram of fish tissue (P_f), we require values of the mass of a [^{14}C]*n*PS (m_p), which are obtained from the product of the particle's density (ρ_p) and volume (V_p). Given that $\rho_p = 0.96$ g cm^{-3}, $V_{p,\,20\text{ nm}} = 4.19 \cdot 10^3$ nm^3, and $V_{p,\,250\text{ nm}} = 8.18 \cdot 10^6$ nm^3, the values for m_p are $4.02 \cdot 10^{-9}$ ng and $7.85 \cdot 10^{-6}$ ng for the 20 nm and 250 nm particles, respectively. The particle concentration in fish (particles $g_{w.w.}^{-1}$) is then calculated with:

$$P_f\ [\text{particles}\ g_{w.w.}^{-1}] = \frac{C_{\text{mass}}\ [\text{ng}\ g_{w.w.}^{-1}]}{m_p\ [\text{ng}\ particle^{-1}]} = \frac{C_{\text{mass}}\ [\text{ng}\ g_{w.w.}^{-1}]}{\rho_p \cdot V_p} \tag{S2}$$

Text S3: Toxicokinetic Modelling.

Uptake–Elimination Model and Assumptions

Toxicokinetic (TK) modelling of [^{14}C]*n*PS uptake and elimination in rainbow trout was performed using the *MOdeling and StAtistical tools for ecotoxICology* (**MOSAIC$_{bioacc}$**) framework[5]. This tool, developed within a Shiny environment[6], and hosted at the Rhône-Alpes Bioinformatics Center[7], is freely accessible via the web platform https://mosaic.univ-lyon1.fr/bioacc.

MOSAICbioacc follows EFSA recommendations for transparent and reproducible modelling practices[8]. All input data (CSV format) were prepared, uploaded, and validated according to the user guide (http://lbbe-shiny.univ-lyon1.fr/mosaic-bioacc/data/user_guide.pdf).

The TK framework treats the organism as a single compartment, with first-order uptake and elimination kinetics describing bioaccumulation from food exposure[9]. Fitting plots and parameter estimates— such as the uptake rate via food (k_{uf}, d^{-1}), elimination rates via excretion (k_{ee}, d^{-1}), and bioaccumulation metrics (kinetic and steady-state biomagnification factors, BMF_k and BMF_{ss}) — were generated alongside standard goodness-of-fit statistics (Figures S4-S5).

Model Equations

Uptake and elimination of [^{14}C]*n*PS were described by the following differential equations:

$$\frac{dC_p(t)}{dt} = k_{uf} \cdot C_f - k_{ee} \cdot C_p(t), for\ 0 \le t \le t_c \ (1)$$

$$\frac{dC_p(t)}{dt} = -k_{ee} \cdot C_p(t), for\ t \ge t_c \ (2)$$

where Cp is the internal concentration of *n*PS in the fish at time t (µg $g_{w.w.}^{-1}$), t is the time (day), k_{uf} is the uptake rate constant related to the food (mL g^{-1} day^{-1}), C_f is the concentration in the food (µg $g_{w.w.}^{-1}$), k_{ee} is the depuration rate constant related to excretion process (day^{-1}), and t_c is the duration of the accumulation phase.

The bioconcentration factor (BCF) and **biological half-life** were calculated as follows:

$$BCF = \frac{k_u}{k_{ee}} \ (3)$$

$$t_{1/2} = \frac{\ln 2}{k_{ee}} \ (4)$$

This kinetic model was produced using the free and open-access TK modelling tools MOSAIC web service (http://umr5558-shiny.univ-lyon1.fr/mosaic-bioacc/) developed by Ratier et al.[9] and Charles et al.[10]. MOSAIC allows for the simultaneous consideration of different exposure routes and several elimination processes, automatically adapting the fitted TK model according to the input experimental data.

Parameter Priors, MCMC Settings, and Model Validation

Model parameters were estimated using Bayesian inference with Markov Chain Monte Carlo (MCMC) sampling implemented in MOSAIC$_{bioacc}$. Default prior distributions were applied to all kinetic

parameters, ensuring parameter identifiability while avoiding bias. Convergence was verified through trace plots and posterior diagnostics.

Posterior distributions and fitted curves are presented in Figures S4 and S5, showing strong agreement between observed and modelled values.

This modelling framework enables quantitative estimation of uptake and elimination kinetics while integrating uncertainty propagation, providing a transparent, reproducible, and EFSA-compliant approach for bioaccumulation analysis.

Figure S1. FTIR and Raman spectroscopy analyses of particles.

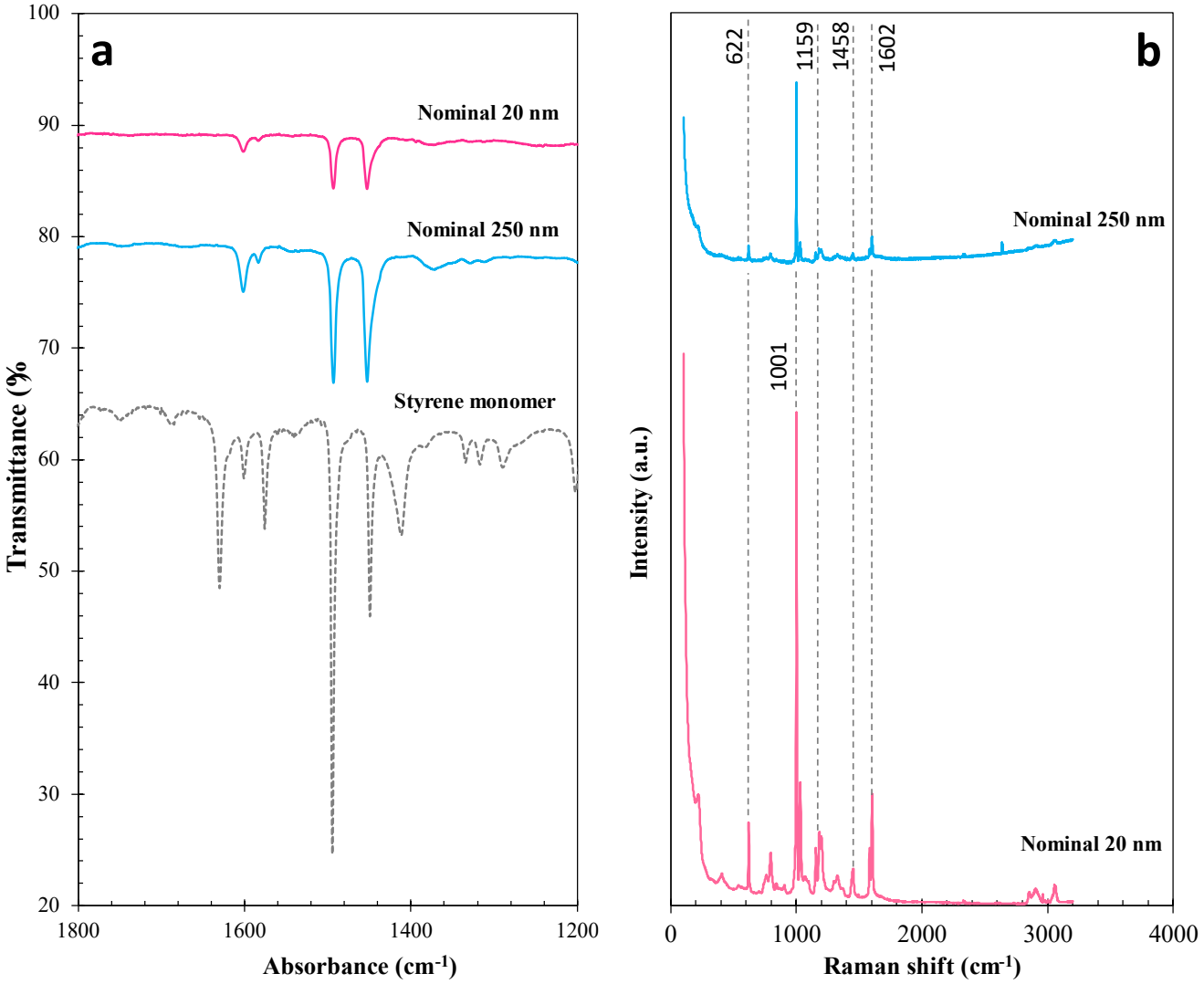

Figure S 1. Composition characterization of nano-polystyrene particles of 20 nm (depicted in pink) and 250 nm (depicted in blue), synthesized through (a) FTIR analysis, wherein the monomer styrene is also represented (dashed black line), and (b) Raman spectroscopy.

Figure S2. Calibration Curves for Quantitative Whole-Body Autoradiography

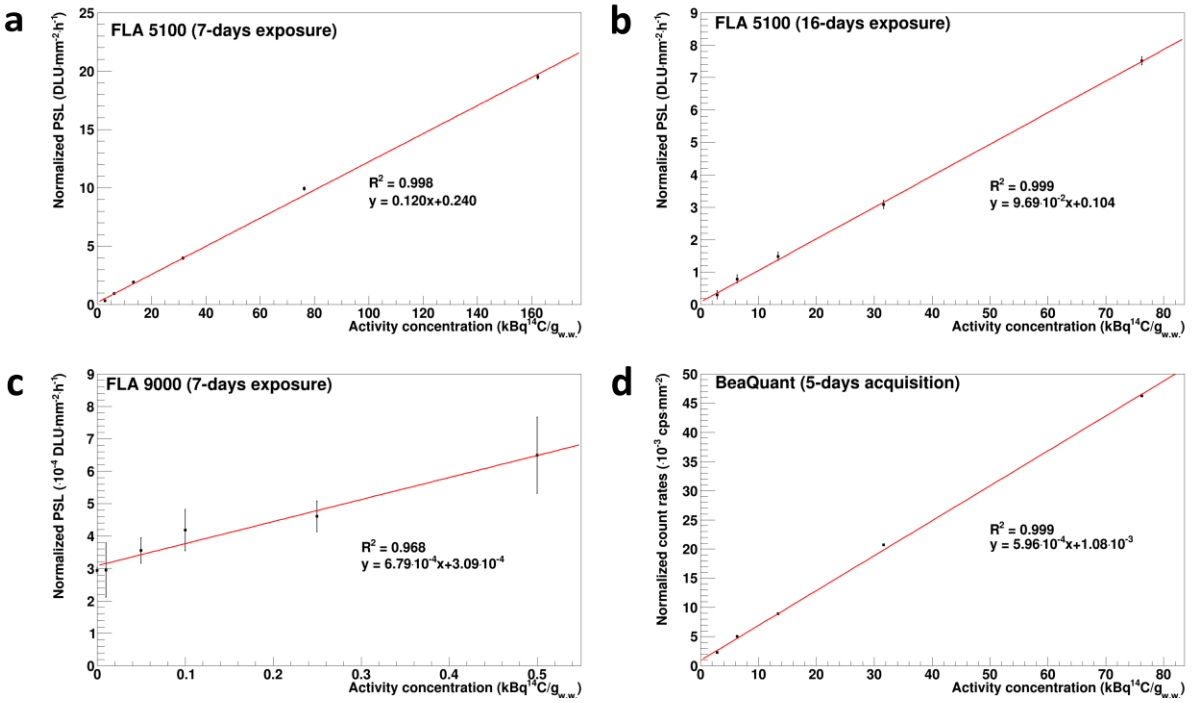

Figure S 2. Linear calibration plot of the autoradiographs collected from the **(a)** FLA-5100 (7-days exposure), **(b)** FLA-5100 (16-days exposure), **(c)** FLA 9000 (7-days exposure), and **(d)** BeaQuant (5-days acquisition), respectively. Data from FLA-5100 and BeaQuant was calibrated against the ^{14}C-PMMA standards, which were converted to activity concentration per unit wet weight of fish (using the Monte Carlo simulated emission fraction and density of the fish organs). Data from FLA 9000 were calibrated against serum standards with a lower activity concentration range (0 to 0.5 kBq ^{14}C $g_{w.w.}^{-1}$). For phosphor screen autoradiography (FLA-5100 and FLA 9000) measurements, the normalized PSL values are expressed in the unit of digital light units per mm^2 per hour. The error bars represent the standard deviation of all the autoradiography data acquired. For the BeaQuant measurements, the normalized count rates are expressed in the unit of counts per second per mm^2. Error bars were calculated using the uncertainty of the counts (square root of total counts per data point).

Figure S3. Comparison of Autoradiograph from BeaQuant and Phosphor Screen Autoradiography

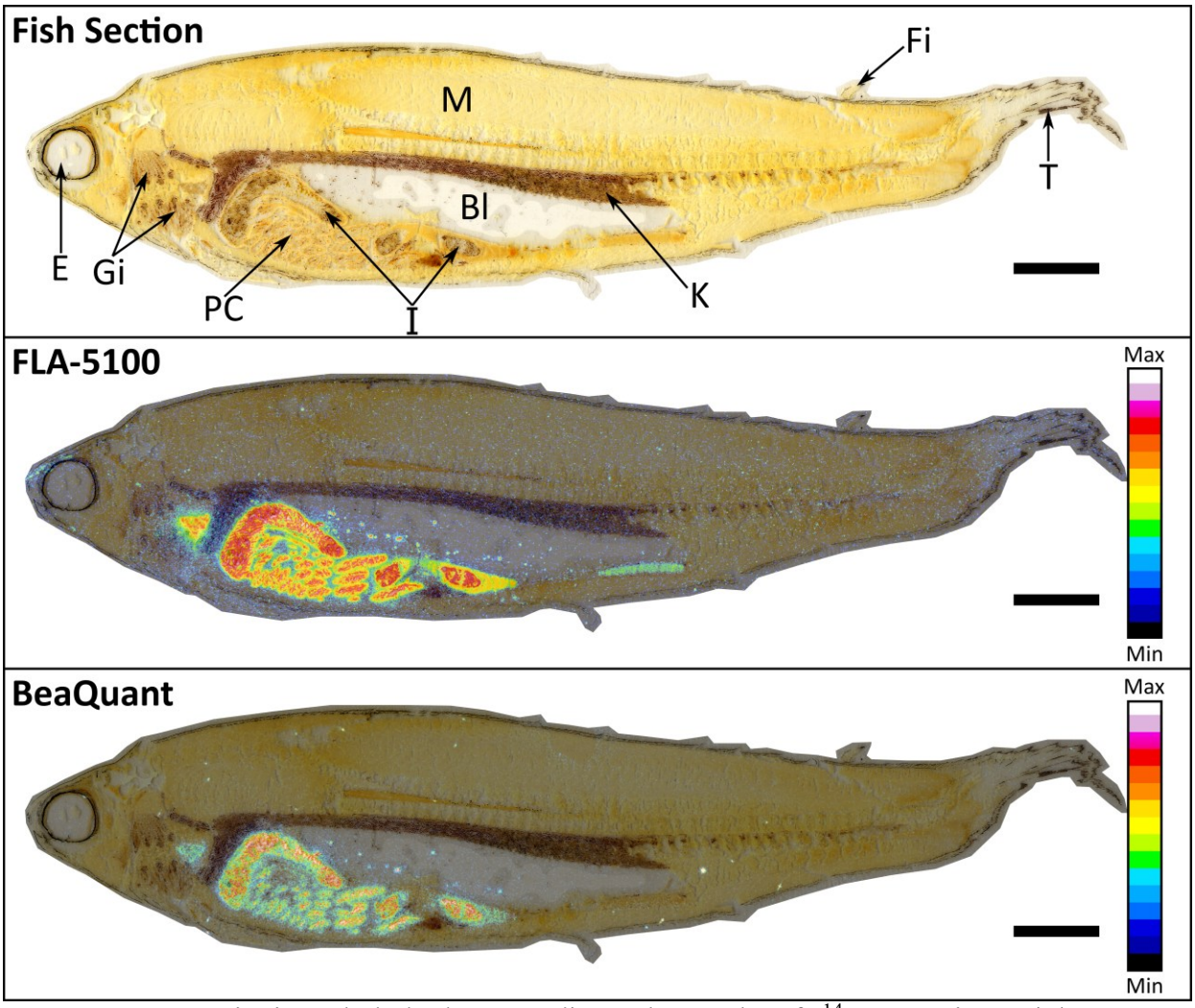

Figure S 3. Quantitative whole-body autoradiography results of [^{14}C]*n*PS$_{20}$ in a rainbow trout section following acute exposure to 250 ppb at 2 days post-ingestion. The BeaQuant acquisition time is 5 days whereas the exposure time for phosphor screen autoradiography is 7 days. In both cases, the autoradiograph is overlaid onto the image of the fish section using Inkscape. The scale bar represents 1 cm. The colour scale is normalized, with the minimum as the limit of detection and the maximum is within the linearity of the standards calibration. Similar to figure S1, an inverted colour scale was used to prevent misinterpretation of data from the natural colour of the fish. Abbreviations used are: Bl (air bladder), E (Eye), Fi (Fins), Gi (Gills), I (intestine), K (Kidney), M (Muscle), PC (Pyloric Caeca), T (Tail).

Figure S4. Mosaic Bioacc modelling for tissue analyses.

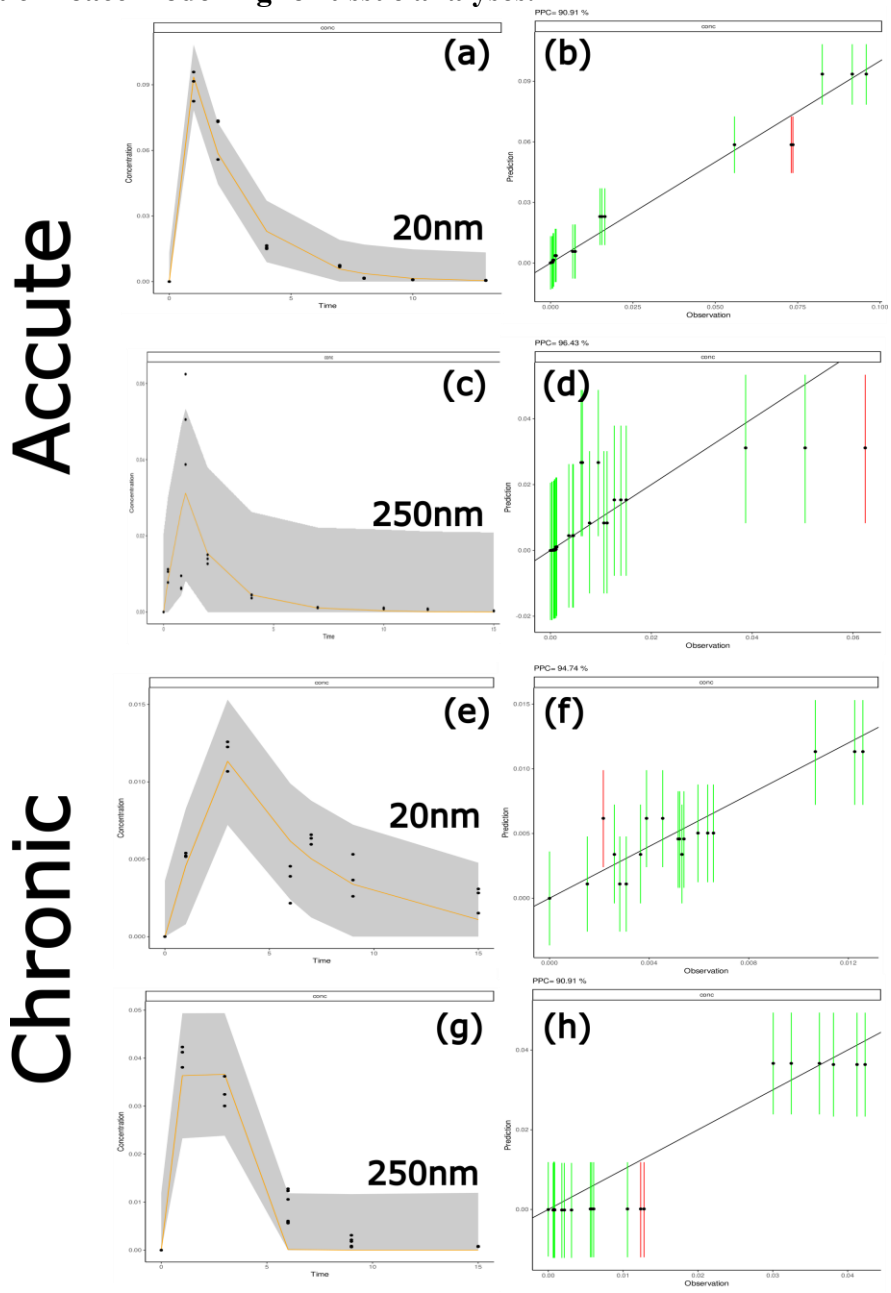

Figure S 4. Mosaic Bioacc modelling for tissue analyses. (a), (c), (e), (g) Measured (black dots) and predicted contaminant concentrations in the organism ($\mu g.g^{-1}$). Median predictions are symbolized by the orange plain line and the uncertainty bands by the gray zone which is delimited by the 2.5% and 97.5% quantiles in orange dotted lines. (b), (d), (f) and (h) are Goodness-of-fit criteria are given using the Posterior Predictive Check (PPC). The PPC shows the observed values against their corresponding estimated predictions (black dots), along with their 95% credible interval (vertical segments). If the fit is correct, we expect to see 95% of the data within the intervals. Ideally, observations and predictions should coincide, so we would expect to see black dots along the first bisector $y = x$ (plain black line). The 95% credible intervals are coloured in green if they overlap this line, in red otherwise.

Figure S5. Mosaic Bioacc modelling for feaces analyses.

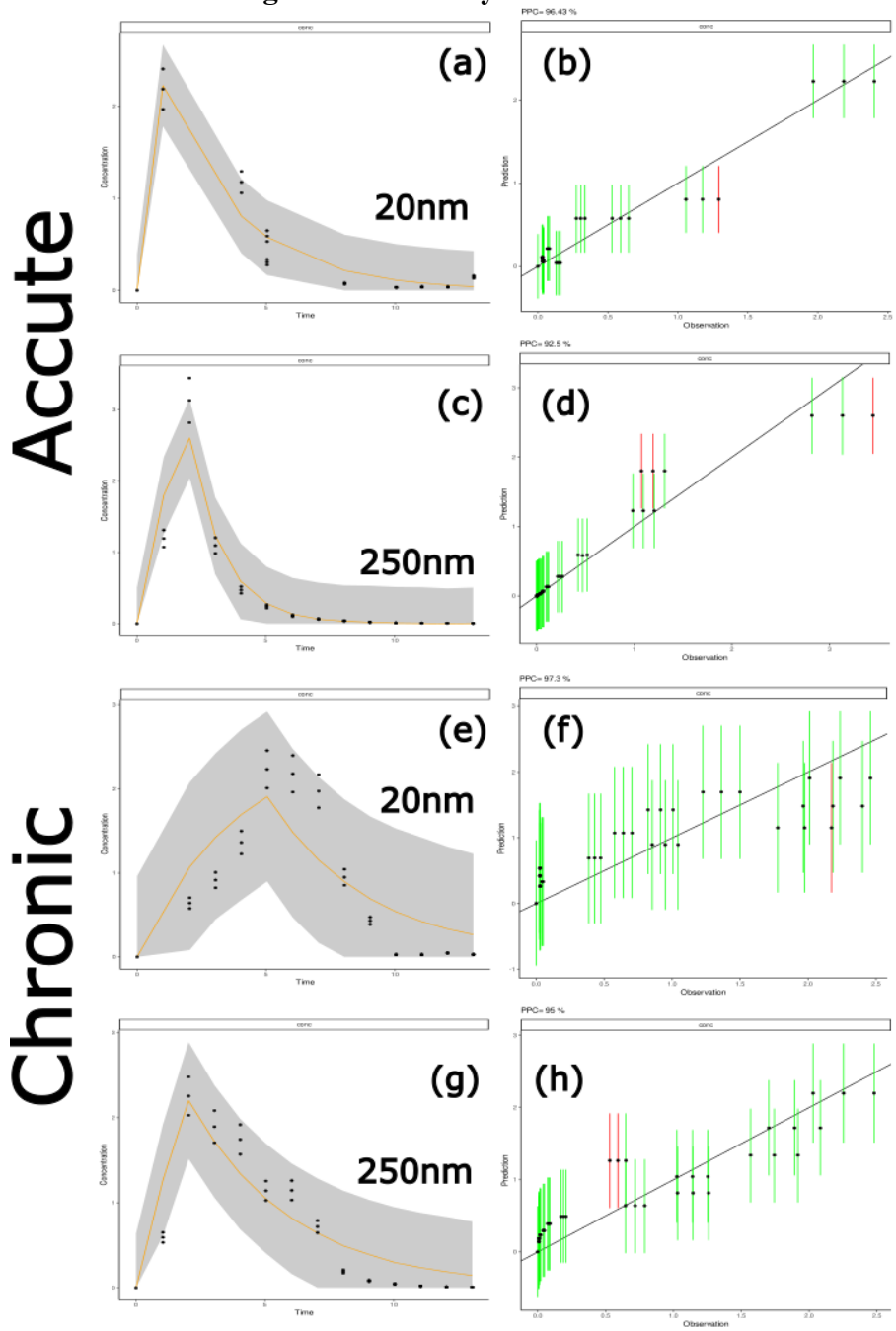

Figure S 5. Mosaic Bioacc modelling for feaces analyses. (a), (c), (e), (g) Measured (black dots) and predicted contaminant concentrations in the organism ($\mu g.g^{-1}$). Median predictions are symbolized by the orange plain line and the uncertainty bands by the gray zone which is delimited by the 2.5% and 97.5% quantiles in orange dotted lines. (b), (d), (f) and (h) are Goodness-of-fit criteria are given using the Posterior Predictive Check (PPC). The PPC shows the observed values against their corresponding estimated predictions (black dots), along with their 95% credible interval (vertical segments). If the fit is correct, we expect to see 95% of the data within the intervals. Ideally, observations and predictions should coincide, so we would expect to see black dots along the first bisector $y = x$ (plain black line). The 95% credible intervals are coloured in green if they overlap this line, in red otherwise.

Figure S6. Autoradiography of Rainbow Trout after Acute Exposure (250 ppb) to 250 nm [^{14}C]*n*PS

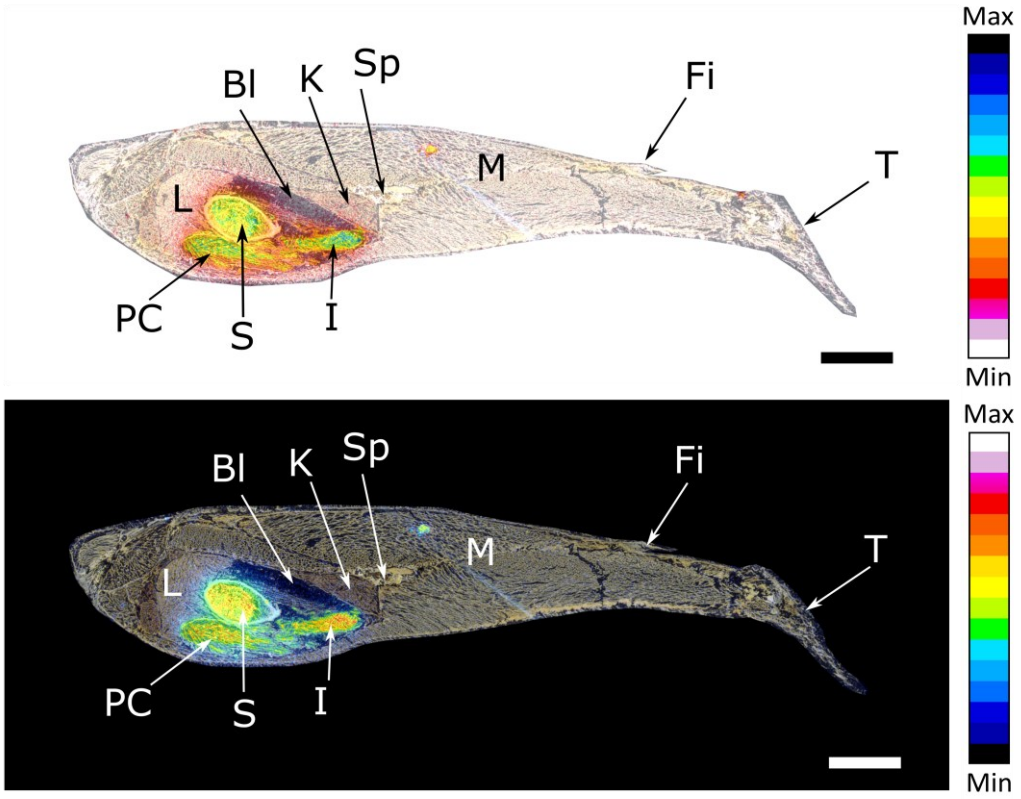

Figure S 6. Quantitative whole-body autoradiography (16-days exposure) results of [^{14}C]*n*PS$_{250}$ in 4 rainbow trout sections following acute exposure to 250 ppb at 2, 4, 7, and 13 days (from right to left) post-ingestion, respectively. The autoradiographs were overlaid on the fish sections to aid visualization of the distribution in the respective organs. The white scale bar represents 1 cm. The colour scale is normalized, with the minimum as the limit of detection and the maximum is within the linearity of the standards calibration. The top figure shows the autoradiograph in the usual colour scale used in this study. However, to prevent confusion between the natural colour of the fish sections (yellow) and the lower range of the colour scale, we present the autoradiograph with the inverted colour scale on the bottom of the figure. At 16 days of exposure, the results cannot be quantified accurately due to the fading process experienced in phosphor screen autoradiography. The maximum activity concentration found within the sample (27.2 ^{14}C kBq $g_{w.w.}^{-1}$) is below the limit of quantification (LOQ = 38.4 ^{14}C kBq $g_{w.w.}^{-1}$, Table S1). Abbreviations: Bl (air bladder), Fi (Fins), I (intestine), K (Kidney), L (Liver), M (Muscle), PC (Pyloric Caeca), S (Stomach), Sp (Spine), T (Tail).

Figure S7. Physical tissue section photos of of [^{14}C]*n*PS$_{20}$ in *O. mykiss* following acute exposure

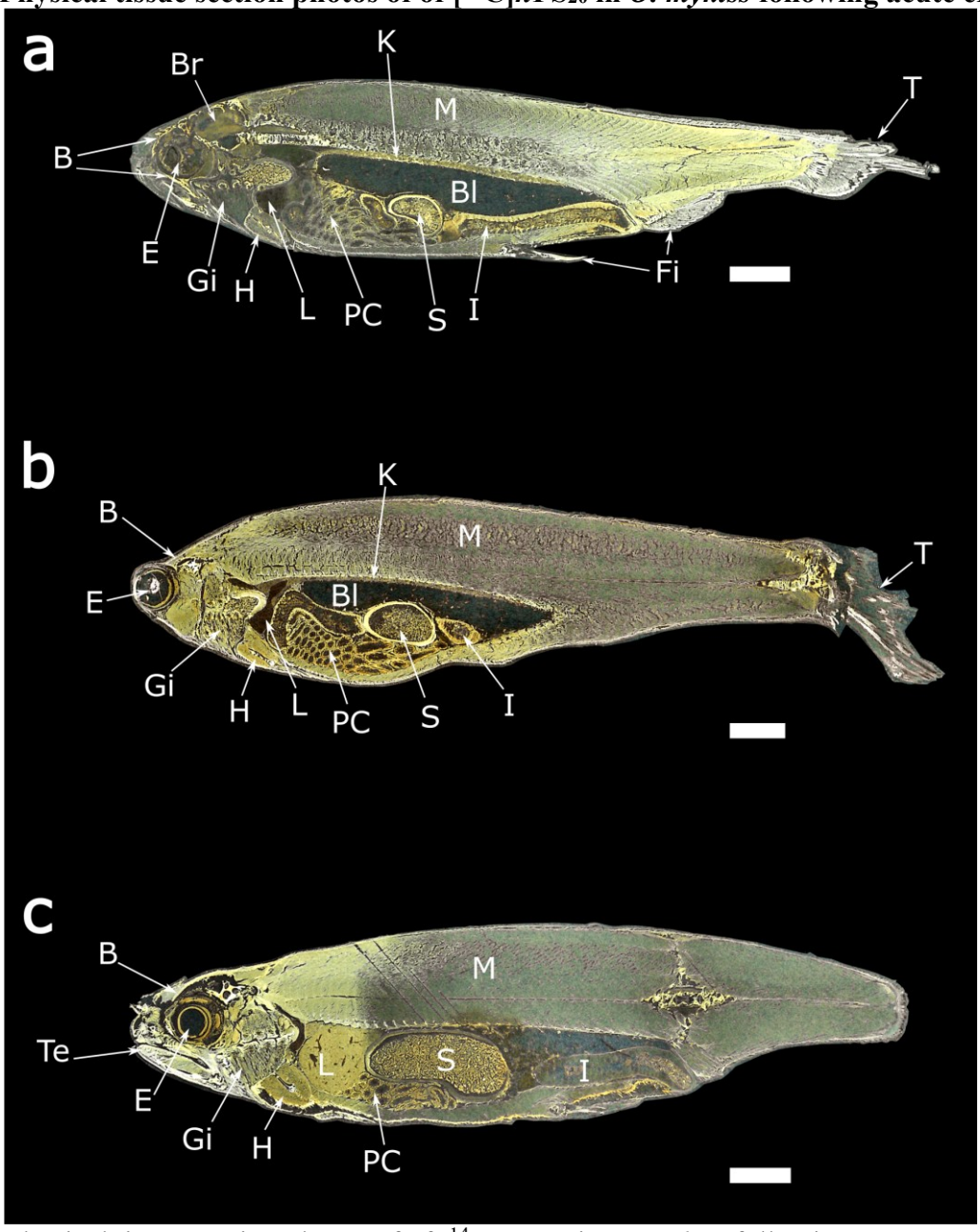

Figure S 7. Physical tissue section photos of of [^{14}C]*n*PS$_{20}$ in *O. mykiss* following acute exposure to 250 ppb at (a) 0.2 day, (b) 1 day, and (c) 4 days post-ingestion. Abbreviations: B (Bone), Bl (air bladder), Br (Brain), E (Eye), Fi (Fins), Gi (Gills), H (Heart), I (intestine), K (Kidney), L (Liver), M (Muscle), PC (Pyloric Caeca), T (Tail), Te (teeth).

Figure S8. Physical tissue section photos of of [^{14}C]*n*PS$_{20}$ in *O. mykiss* following short-term low-dose exposure.

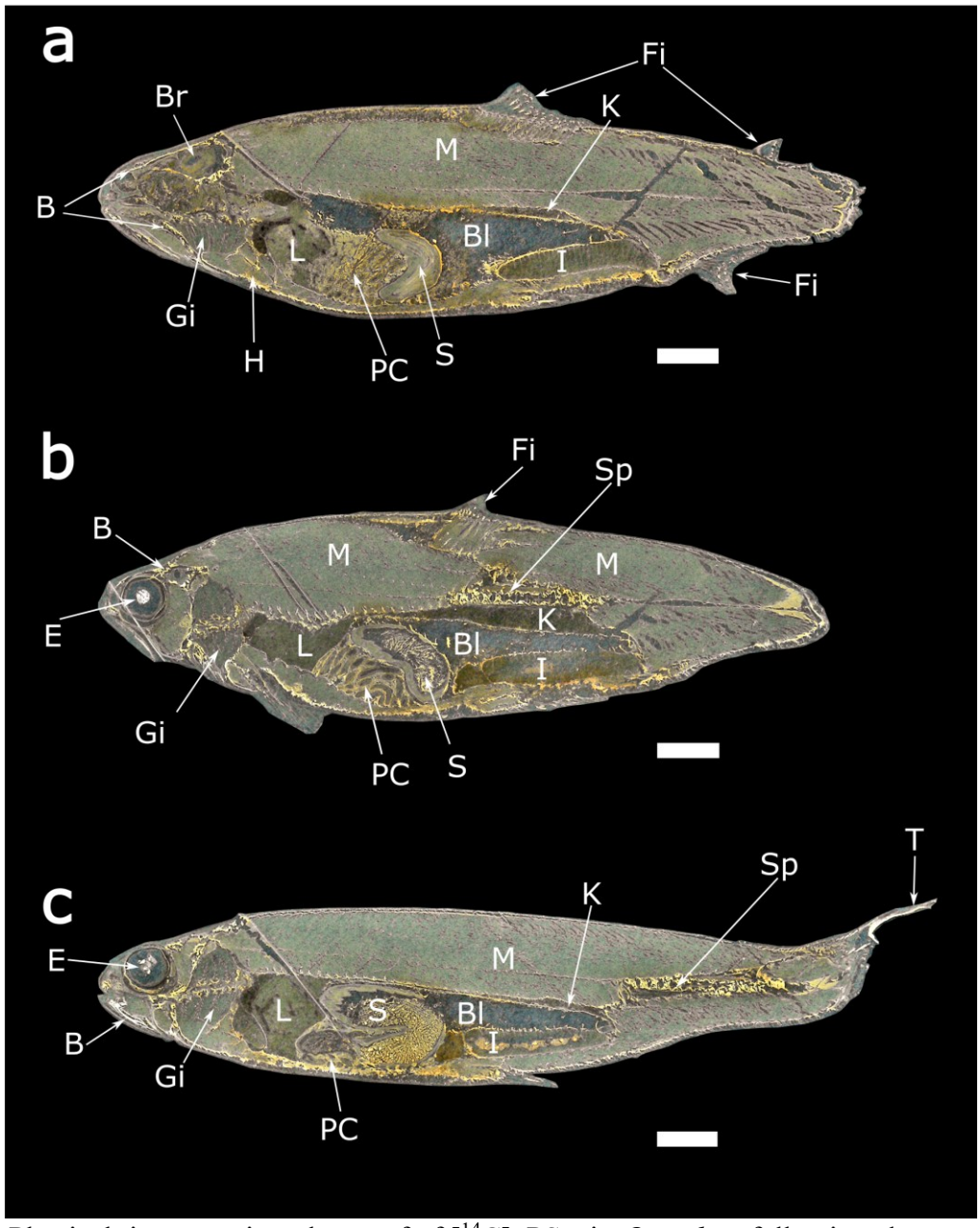

Figure S 8. Physical tissue section photos of of [^{14}C]*n*PS$_{20}$ in *O. mykiss* following short-term low-dose exposure to 8 ppb at (a) 0.2 day, (b) 1 day, and (c) 4 days ingestion. Abbreviations: B (Bone), Bl (air bladder), Br (Brain), E (Eye), Fi (Fins), Gi (Gills), H (Heart), I (intestine), K (Kidney), L (Liver), M (Muscle), PC (Pyloric Caeca), S (stomach), Sp (Spine), T (Tail), Te (teeth).

Figure S9. Physical tissue section photos of of [^{14}C]*n*PS$_{250}$ in *O. mykiss* following short-term low-dose exposure.

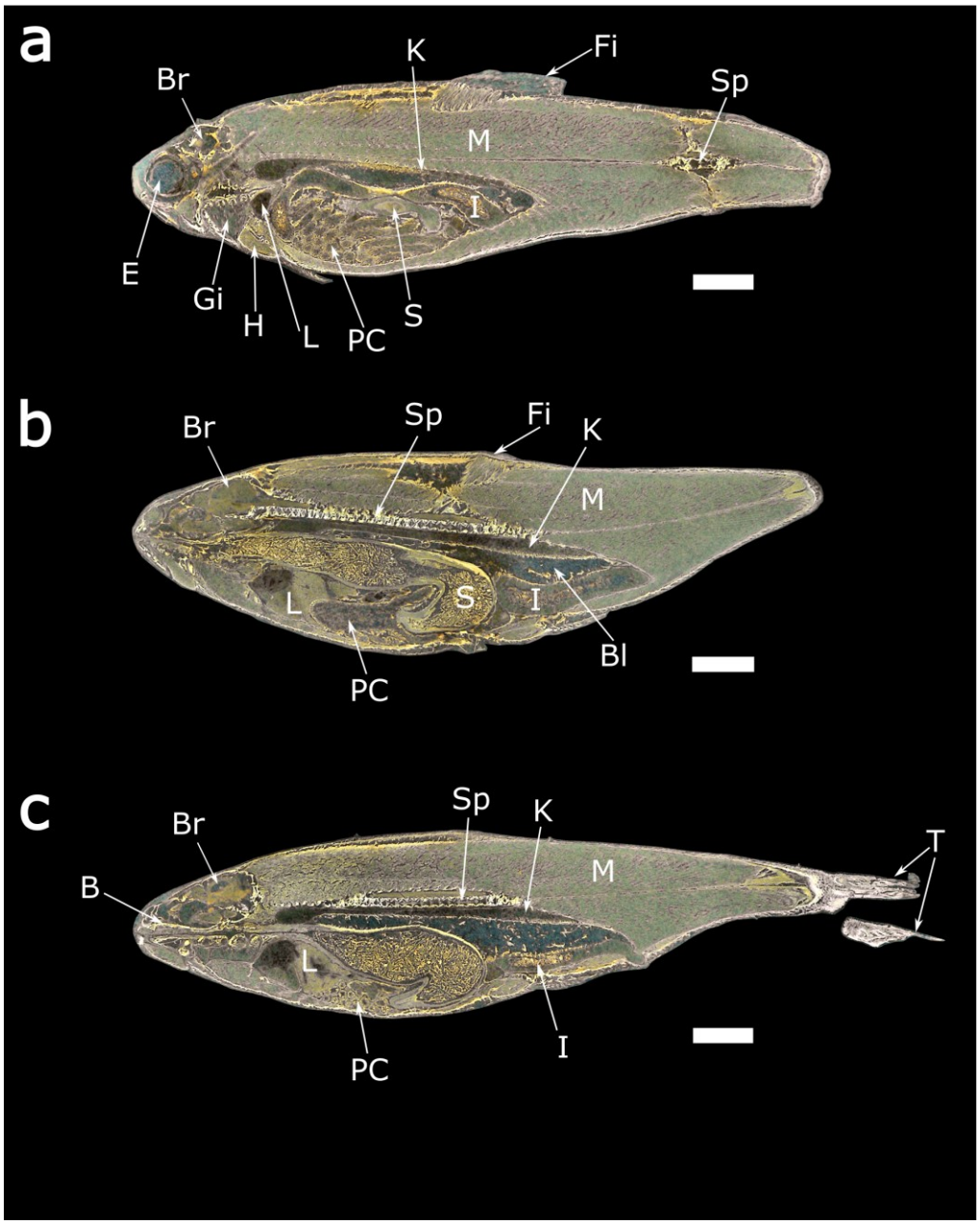

Figure S 9. Physical tissue section photos of of [^{14}C]*n*PS$_{250}$ in *O. mykiss* following short-term low-dose exposure to 8 ppb at (a) 0.2 day, (b) 1 day, and (c) 4 days ingestion. Abbreviations: B (Bone), Bl (air bladder), Br (Brain), E (Eye), Fi (Fins), Gi (Gills), H (Heart), I (intestine), K (Kidney), L (Liver), M (Muscle), PC (Pyloric Caeca), S (stomach), Sp (Spine), T (Tail), Te (teeth).

Table S1. Experimental design and sampling timeline for rainbow trout exposure to [^{14}C]*n*PS

Table S1. Experimental design for [^{14}C]-labelled and unlabelled nanopolystyrene (*n*PS) exposure in juvenile rainbow trout (*Oncorhynchus mykiss*). The table summarises all treatments, nominal particle sizes, exposure concentrations, activity levels, exposure and depuration durations, and sampling regimes. Fish were exposed either to unlabelled controls or to radiolabelled *n*PS under acute (single feeding) or short-term (repeated feeding) scenarios to assess uptake, biodistribution, and depuration kinetics. Each timepoint represents the mean of three fish per replicate tank, with the number of replicates indicated. A total of 324 fish were used across all treatments. Abbreviations: N/A, not applicable; w.w., wet weigth.

Treatment	Nominal size (nm)	Exposure concentration (ng $g_{w.w.}^{-1}$))	Activity (kBq $g_{w.w.}^{-1}$)	Exposure type	Exposure duration	Depuration duration (day)	Sampling timepoint		No. fish per timepoint	Replicates (tanks)	Number of fish	Purpose / Notes
							total ^{14}C/LSC (day)	^{14}C tissue distribution/QWBA (day)				
Control (blank feed)	–	0	0	Particle free feed	N/A	15d	1, 3, 6, 7, 9, 12, 15	1, 3, 6, 7, 9, 12, 15	2	1	28	Baseline endogenous ^{14}C; check background activity
Control Acute (un-labelled PSNPs)	20 & 250	250	0	Single ^{12}C feeding	24 h	13d	1, 2, 4, 7, 8, 10, 13	1, 2, 4, 7, 8, 10, 13	2	1	28	Verify absence of artefacts from polymer matrix
Control Short-term (un-labelled PSNPs)	20 & 250	8 per day	0	Single ^{12}C feeding	5 d	15d	1, 3, 6, 7, 9, 12, 15	1, 3, 6, 7, 9, 12, 15	2	1	28	Verify absence of artefacts from polymer matrix
Acute high dose	20	250	14.8	Single ^{14}C feeding	24 h	13d	0.2, 0.8, 1, 2, 4, 7, 8, 10, 13	1, 2, 4, 7, 8, 10, 13	2	2	(32x2) 64	Assess short-term uptake and tissue distribution
Acute high dose	250	250	14.8	Single ^{14}C feeding	24 h	13d	0.2, 0.8, 1, 2, 4, 7, 8, 10, 13	1, 2, 4, 7, 8, 10, 13	2	2	(32 x 2) 64	Compare size-dependent kinetics (nanoscale vs sub-µm)
Short-term low dose	20	8 per day	4.1 per day	Daily ^{14}C feeding	5 days	15d	1, 3, 6, 7, 9, 12, 15	1, 3, 6, 7, 9, 12, 15	2	2	(28 x 2) 56	Evaluate cumulative uptake and depuration
Short-term low dose	250	8 per day	4.1 per day	Daily ^{14}C feeding	5 days	15d	1, 3, 6, 7, 9, 12, 15	1, 3, 6, 7, 9, 12, 15	2	2	(28 x 2) 56	Compare clearance and retention patterns

Notes:
- All fish (mean weight = 17 ± 2 g) were fasted 24 h prior to exposure.
- Each treatment used independent tanks supplied with aerated, temperature-controlled freshwater (12 ± 1 °C).
- Activity values correspond to total ^{14}C disintegrations per gram wet tissue in feed; uncertainties ≤ 5 %.
- Data from replicate tanks were pooled for kinetic modelling once no tank effect was detected (ANOVA, $p > 0.05$).
- During the depuration period, fish were fed daily with commercial pellet

Table S2: Calculated Limits of Detection and Quantification of the Techniques Used

Table S 2. Summary of the limits of detection (LOD) and quantification (LOQ) for the FLA 9000, FLA-5100, and the BeaQuant system, respectively. The values are reported in terms of activity concentration and nanopolystyrene particle mass concentration (per wet weight of fish tissue) and rounded up to 3 significant figures. For the FLA and LSC techniques, the LOD is calculated by multiplying the standard deviation of the background by 3.3, and the LOQ was set at 10 times the standard deviation of the blank measurements. Specifically, for the FLA measurements, we derived the standard deviations of the y-intercept from the calibration plots in Figure S3. For the LSC, the standard deviation was calculated after performing measurements on 10 blank replicates. On the other hand, for the BeaQuant technique, the LOD is calculated by inputting a blank sample measurement into a modified Currie equation, following Ang et al[11], while the LOQ is derived by multiplying the LOD by 3.

Detector	Exposure Time (days)	LOD		LOQ	
		(^{14}C kBq $g_{w.w.}^{-1}$)	(ng $g_{w.w.}^{-1}$)	(^{14}C kBq $g_{w.w.}^{-1}$)	(ng $g_{w.w.}^{-1}$)
FLA 9000	7	$6.98 \cdot 10^{-2}$	3.31	$2.12 \cdot 10^{-1}$	10.1
FLA-5100	7	$2.02 \cdot 10^{-2}$	$9.53 \cdot 10^{-1}$	$6.10 \cdot 10^{-2}$	2.89
	16	12.7	$6.00 \cdot 10^{2}$	38.4	$1.82 \cdot 10^{3}$
BeaQuant	5	$6.94 \cdot 10^{-1}$	32.9	2.08	98.6
LSC (Hidex 300)	N.A.	$6.62 \cdot 10^{-5}$	$3.14 \cdot 10^{-3}$	$1.82 \cdot 10^{-2}$	$8.62 \cdot 10^{-3}$

Table S3: Elemental Composition of Monte Carlo Simulated Rainbow Trout Organs

Table S 3. Elemental composition of each simulated material (by atomic composition). This information was obtained from the GEANT4 material database and the ICRP110 human phantom model[12,13].

Simulated Material	Elemental Composition											
	H	**C**	**N**	**O**	**Na**	**P**	**S**	**Cl**	**K**	**Mg**	**Ca**	**Fe**
G4_BRAIN_ICRP	0.107	0.145	0.022	0.712	0.002	0.004	0.002	0.003	0.003	-	-	-
ICRP110 Phantom Male Oesophagus	0.104	0.213	0.029	0.644	0.001	0.002	0.003	0.002	0.002	-	-	-
G4_EYE_LENS_ICRP	0.096	0.195	0.057	0.646	0.001	0.001	0.003	0.001	-	-	-	-
ICRP110 Phantom Male Heart	0.104	0.138	0.029	0.719	0.001	0.002	0.002	0.002	0.003	-	-	-
ICRP110 Phantom Male Kidneys	0.103	0.124	0.031	0.731	0.002	0.002	0.002	0.002	0.002	-	0.001	-
ICRP110 Phantom Male Liver	0.102	0.130	0.031	0.725	0.002	0.002	0.003	0.002	0.003	-	-	-
G4_MUSCLE_SKELETAL_ICRP	0.102	0.143	0.034	0.710	0.001	0.002	0.003	0.001	0.004	-	-	-
ICRP110 Phantom Male Stomach	0.105	0.114	0.025	0.750	0.001	0.001	0.001	0.002	0.001	-	-	-
ICRP110 Phantom Male Large Intestines	0.105	0.113	0.026	0.750	0.001	0.001	0.001	0.002	0.001	-	-	-
G4_BONE_CORTICAL_ICRP	0.034	0.155	0.042	0.435	0.001	0.103	0.003	-	-	0.002	0.225	-
ICRP110 Phantom Male Spleen	0.102	0.111	0.033	0.743	0.001	0.002	0.002	0.003	0.002	-	-	0.001
G4_TESTIS_ICRP	0.106	0.099	0.020	0.766	0.002	0.001	0.002	0.002	0.002	-	-	-

Table S4: Parameter estimates from Mosaic Bioacc plateform.

Table S 4. Parameter medians (50% quantile) with estimates for k_{ee} and biomagnification factors (BMF) are given as probability distributions.

		k_u *day*$^{-1}$	k_{ee} *day*$^{-1}$	BMF_k	BMF_{ss}	$t_{1/2}$ *day*	$t_{95\%}$ *day*
		Tissue					
20 nm Acute	Average	0.47	0.47	1.00	0.37	1.48	6.40
	SD	0.02	0.04	0.06	0.03	17.29	74.74
250 nm acute	Average	0.21	1.17	0.27	0.12	0.59	2.56
	SD	0.75	9.60	0.09	0.05	0.07	0.31
20 nm short-term	Average	0.63	0.20	3.16	1.41	3.41	14.76
	SD	0.08	0.04	0.39	0.26	17.80	76.92
250 nm short-term	Average	244.71	53.60	4.58	4.58	0.01	0.06
	SD	269.86	59.04	0.32	0.81	0.01	0.05
		Faeces					
20 nm Acute	Average	10.47	0.33	31.40	8.90	2.07	8.96
	SD	0.59	0.03	2.02	0.90	26.37	113.97
250 nm acute	Average	9.99	0.75	13.32	10.40	0.92	3.98
	SD	0.76	0.07	0.71	1.12	9.75	42.12
20 nm short-term	Average	172.49	0.25	693.98	275.14	2.78	12.01
	SD	12.45	0.02	45.39	43.52	29.81	128.84
250 nm short-term	Average	84.32	0.25	333.66	238.75	2.72	11.76
	SD	10.45	0.04	30.00	63.64	18.08	78.13

Table S5: Emission Fraction of ^{14}C from Different Rainbow Trout Organs

Table S 5. Summary of the rainbow trout organ's tissue density, its referenced analogous human organ, and the calculated emission fraction (F_E). The swim bladder was omitted in our simulations as it mainly consists of gas, which has insignificant contributions to the autoradiograph due to the slicing of the sections (large regions of air pockets without any tissue present). The F_E values were rounded to 3 significant figures.

Rainbow Trout Organs	Density (g cm^{-3})	Analogous Simulated Material	F_E
Brain	1.04	G4_BRAIN_ICRP	0.275
Oesophagus	1.03	ICRP110 Phantom Male Oesophagus	0.276
Eyes	1.07	G4_EYE_LENS_ICRP	0.272
Heart	1.05	ICRP110 Phantom Male Heart	0.273
Kidneys	1.05	ICRP110 Phantom Male Kidneys	0.275
Liver	1.05	ICRP110 Phantom Male Liver	0.274
Muscle	1.05	G4_MUSCLE_SKELETAL_ICRP	0.274
Pyloric caeca	1.04	ICRP110 Phantom Male Stomach	0.274
Rectum	1.04	ICRP110 Phantom Male Large Intestines	0.276
Skeleton	1.92	G4_BONE_CORTICAL_ICRP	0.206
Spleen	1.04	ICRP110 Phantom Male Spleen	0.275
Testicle	1.04	G4_TESTIS_ICRP	0.275

References

(1) Donnard, J.; Berny, R.; Carduner, H.; Leray, P.; Morteau, E.; Provence, M.; Servagent, N.; Thers, D. The Micro-Pattern Gas Detector PIM: A Multi-Modality Solution for Novel Investigations in Functional Imaging. *Nucl Instrum Methods Phys Res A* 2009, *610* (1), 158–160. https://doi.org/10.1016/j.nima.2009.05.186.

(2) Donnard, J.; Thers, D.; Servagent, N.; Luquin, L. High Spatial Resolution in β-Imaging with a PIM Device. *IEEE Trans Nucl Sci* 2009, *56* (1). https://doi.org/10.1109/TNS.2008.2005673.

(3) Delayre, C.; Sammaljärvi, J.; Billon, S.; Muuri, E.; Sardini, P.; Siitari-Kauppi, M. Comparison of Phosphor Screen Autoradiography and Micro-Pattern Gas Detector Based Autoradiography for the Porosity of Altered Rocks. *Sci Rep* 2020, *10*, 9455. https://doi.org/10.1038/s41598-020-65791-7.

(4) Skrable, K.; Chabot, G.; French, C. World Atmospheric CO2, Its 14C Specific Activity, Non-Fossil Component, Anthropogenic Fossil Component, and Emissions (1750-2018). *Health Phys* 2022, *122* (2), 291–305. https://doi.org/10.1097/HP.0000000000001485.

(5) Charles, S.; Veber, P.; Delignette-Muller, M. L. MOSAIC: A Web-Interface for Statistical Analyses in Ecotoxicology. *Environmental Science and Pollution Research* 2018, *25* (12), 11295–11302. https://doi.org/10.1007/s11356-017-9809-4.

(6) Chang, S.; Cheng, W.; Allaire, J. J.; Xie, Y.; McPherson, J. Shiny: Web Application Framework for R. Version 1.5.0. rstudio 2020. http://shiny.rstudio.com/ (accessed 2024-06-17).

(7) PRABI. *Rhône-Alpes Bioinformatics Center*. Rhône-alpes bioinformatics center. http://www.prabi.fr (accessed 2024-06-17).

(8) European Food Safety Authority (ESFA) PPR Panel. Scientific Opinion on Good Modelling Practice in the Context of Mechanistic Effect Models for Risk Assessment of Plant Protection Products. *EFSA Journal* 2014, *12* (3). https://doi.org/10.2903/j.efsa.2014.3589.

(9) Ratier, A.; Lopes, C.; Multari, G.; Mazerolles, V.; Carpentier, P.; Charles, S. New Perspectives on the Calculation of Bioaccumulation Metrics for Active Substances in Living Organisms. *Integr Environ Assess Manag* 2022, *18* (1), 10–18. https://doi.org/10.1002/ieam.4439.

(10) Charles, S.; Ratier, A.; Baudrot, V.; Multari, G.; Siberchicot, A.; Wu, D.; Lopes, C. Taking Full Advantage of Modelling to Better Assess Environmental Risk Due to Xenobiotics—the All-in-One Facility MOSAIC. *Environmental Science and Pollution Research* 2022, *29* (20), 29244–29257. https://doi.org/10.1007/s11356-021-15042-7.

(11) W. L. Ang, J.; Bongrand, A.; Duval, S.; Donnard, J.; Parkkonen, J.; Utsunomiya, S.; Koivula, R.; Siitari-Kauppi, M.; T. W. Law, G. Improved Radio-Cesium Detection Using Quantitative Real-Time Autoradiography. *ACS Omega* 2023, *8* (25), 22523–22535. https://doi.org/10.1021/acsomega.3c00728.

(12) International Commission on Radiological Protection; International Commission on Radiation Units and Measurements. *Annals of the ICRP Publication 110: Adult Reference Computational Phantoms*; Polestar Wheatons Ltd, 2009.

(13) Geant4. *Geant4 Material Database*. https://geant4-userdoc.web.cern.ch/UsersGuides/ForApplicationDeveloper/html/Appendix/materialNames.html (accessed 2022-09-22).